[*Reprinted from* THE AERONAUTICAL JOURNAL OF THE ROYAL AERONAUTICAL SOCIETY, *FEBRUARY 1998*]

Computation, analysis and theory of two-phase flows

A. Guha
Department of Aerospace Engineering
University of Bristol
Bristol, UK

PRINTED BY MANOR PARK PRESS LIMITED, EDISON ROAD, HAMPDEN PARK, EASTBOURNE, SUSSEX, ENGLAND
AND PUBLISHED BY THE ROYAL AERONAUTICAL SOCIETY, 4 HAMILTON PLACE, LONDON W1V 0BQ, ENGLAND

Computation, analysis and theory of two-phase flows

A. Guha
Department of Aerospace Engineering
University of Bristol
Bristol, UK

ABSTRACT

The non-equilibrium fluid mechanics and thermodynamics of two-phase vapour–droplet and gas-particle flow are considered. The formation of the droplets as well as their subsequent interaction with the vapour are discussed. Five topics have been given particular attention: (*i*) CFD application to unsteady condensation waves, (*ii*) CFD application to shock waves moving through a vapour–droplet mixture, (*iii*) a new theory of nucleation of water droplets in steam turbines based on Monte Carlo simulation (steam turbines are responsible for 80% of global electricity production and the presence of moisture significantly reduces the turbine efficiency costing £50m per annum in the UK alone), (*iv*) a unified theory for the interpretation of total pressure and total temperature in two-phase flows and, (*v*) a unified theory of particle transport in a turbulent flowfield.

NOMENCLATURE

D_B	Brownian diffusion coefficient
D_T	coefficient of temperature gradient-dependent diffusion
F_S	Saffman lift force
g	acceleration due to gravity
G_E	electrical force
L	characteristic length
$M_{f\infty}$	frozen Mach number at far upstream
p	static pressure
p_0	inlet stagnation pressure; non-equilibrium total pressurer
p_{0e}	equilibrium total pressure
p_{0f}	frozen total pressure
r	droplet radii
R_p	non-dimensional total pressure
S_t	Stokes number
ΔT	subcooling; separate definition in Section 6.3
T_0	inlet stagnation temperature
T_g	vapour temperature
T_s	saturation temperature at local pressure
u^*	friction velocity
V_∞	unperturbed velocity
V^+_{dep}	non-dimensional deposition velocity
$\overline{V}^c_{py}$	particle convective velocity in the y-direction
$\overline{V}_f$	average fluid velocity
$\overline{V}_p$	average particle velocity
δ	ratio of specific heats of the solid and gas
ε	eddy momentum diffusivity
ν	kinematic viscosity
$\overline{\rho}_p$	average particle concentration
τ_D	droplet temperature relaxation time
τ_I	inertial relaxation time
τ_T	vapour thermal relaxation time
τ^+	non-dimensional inertial relaxation time

1.0 INTRODUCTION

The two phase flow of a vapour–liquid mixture consisting of a large number of minute liquid droplets uniformly dispersed throughout a background vapour phase continuum is both scientifically interesting and of engineering importance (in a variety of areas in mechanical, chemical and aerospace engineering, and, meteorology). Similarly, two-phase gas-solid particle flows are important in many industrial processes, environmental engineering and physiology. In the present paper we discuss the formation of the liquid droplets as well as the impact of the droplets or solid particles on the thermo-fluid dynamics of the flow.

What follows is a brief description, with only a few equations, of some of the work with which the present author has been involved over the past few years. The cited references[1-10] give fuller treatment of these topics. The VKI lecture series[1] treats most of these topics together at a much greater depth than that which could be presented in this short paper. It also contains a good repertoire of references and works of many researchers in this field which we do not reproduce here for reasons of economy of space.

2.0 THERMO-FLUID DYNAMICS OF CONDENSATION

2.1 Physical description of homogeneous condensation

All condensing (or evaporating) flows are non-equilibrium to a greater or lesser extent. Departures from equilibrium are measured by the subcooling ΔT which is the difference between the saturation

Paper No. 2266. Manuscript received 5 February 1997, revised version received 1 September 1997, accepted 24 September 1997.

temperature at local pressure and the actual vapour temperature ($\Delta T = T_s - T_g$). ΔT governs the rate at which nuclei are formed as well as the rate at which established droplets grow (or evaporate).

As pure, clean steam expands through a nozzle or a turbine blade passage, droplets do not appear as soon as the condition line crosses the saturation line. This is due to the existence of a free-energy barrier involved in creating new surface area. For some considerable time during expansion the steam remains dry in a metastable equilibrium until the subcooling becomes high enough to trigger an appreciable nucleation rate. Depending on the rate of expansion and the pressure, steam may become subcooled by 30°C-40°C while still remaining dry. The nucleation process leads to the formation of very large numbers (10^{14}-10^{17} nuclei per kg of steam) of tiny droplets (diameter < 1 nm), called the primary fog, more or less uniformly distributed in the continuous vapour phase. Nucleation is practically terminated at the point of maximum subcooling called the Wilson Point. For pure steam, if the Wilson points for tests with varying nozzle inlet conditions are plotted on the equilibrium Mollier diagram, they are contained within a narrow zone around a line called the Wilson line (which corresponds to approximately 3-4% equilibrium wetness line).

The droplets thus formed then rapidly grow in size by exchanging heat and mass with the surrounding, subcooled vapour (the final droplet radii, r, in laboratory nozzles lie in the range 0·02-0·2 μm). The high rate of heat release as a result of rapid condensation, causes a sharp increase in vapour temperature and consequently an exponential decay of the subcooling. Depending on the values of the flow parameters, the initial growth phase of the droplets may give rise to a gradual increase in pressure known as "condensation shock". The term "shock", however, is a misnomer. Although pressure rises as a result of heat addition to supersonic flow, the Mach number downstream of the condensation zone usually remains above unity and more importantly the rise in pressure is gradual.

In conventional, laboratory nozzle experiments, where (dry saturated or superheated) steam is produced in a boiler, the flow must expand to supersonic velocities for significant subcooling to develop. However, if subcooled steam could be supplied at the nozzle inlet, homogeneous condensation could occur in the subsonic part of the flow. This is possible, for example, in a multistage turbine where steam could become subcooled at the inlet of a blade row as a result of work extraction in previous blade rows. Subsonic condensation would result in a decrease, rather than an increase, in pressure.

Some inlet conditions may give rise to such combinations of flow Mach number and heat release rate that necessitate the formation of a true aerodynamic shock wave inside the condensation zone ("supercritical condensation shock"). Under certain conditions this shock wave may become unstable and propagate towards the nozzle throat. The compressive wave ultimately interferes with the nucleation zone causing a reduction in nucleation rate and hence heat release rate. With the cause of its inception removed, the strength of the wave decreases and the flow again expands through the throat in a shock free manner, thus allowing the whole process to repeat itself. Such unsteady flow is normally observed in pure steam when the inlet stagnation temperature T_0 is close to the saturation temperature at the inlet stagnation pressure p_0. Homogeneous condensation then occurs in the transonic region close to the throat causing the flow instability (the flow domain and boundary conditions remaining fixed).

Keeping p_0 fixed, if T_0 is progressively reduced from superheated to subcooled levels, one encounters different regimes of homogeneous condensation in the order: subcritical condensation (the usual pressure humps characteristic of many condensation experiments), supercritical condensation (with an embedded aerodynamic shock wave), oscillatory condensation and subsonic condensation[2].

After the "condensation shock" the steam generally reverts to near thermodynamic equilibrium at which the temperature of the vapour as well as of the droplets is close to the saturation level. Since the growth of liquid phase takes place by heat transfer through a finite temperature difference between the phases, the process is essentially irreversible and has associated with it a net rise in entropy. In turbines this appears as a reduction in the potential for performing work and is referred to as the Thermodynamic Wetness Loss. This is a major component of the overall wetness loss. A simplistic version of an empirical rule, formulated by Baumann in 1921, states that the efficiency of a steam turbine decreases by 1% for 1% increase in mean wetness fraction. A typical value of the wetness fraction at the exit of a steam turbine in a electricity-generating power plant is 10-12%. Thus, in the last stages, the wetness loss is comparable to the combined effects of the profile, secondary and tip leakage losses. A 1988 estimate by the then UK Central Electricity Generating Board showed that the adverse wet steam effects cost them £50m per year. The global implication is thus quite serious since steam turbines are responsible for about 80% of the world-wide generation of electricity and hence there is a considerable economic incentive for further research.

2.2 Computational fluid dynamics applied to the prediction of unsteady condensation waves

The numerical scheme for the calculation of steady as well as unsteady non-equilibrium wet steam flow has been detailed in[2, 4]. Here, we describe only the outline and highlight some important aspects.

One of the most effective methods of calculation is to write a computational "black-box" which contains the nucleation and droplet growth equations, and the energy equation in its thermodynamic form. Together they furnish the full set of equations that describe completely the formation and growth of liquid droplets in a fluid particle (from a Lagrangian viewpoint) if the pressure-time variation is specified. The pressure-time variation is obtained by time marching solutions of the conservation equations such as Denton's method, extensively used for single-phase calculations in turbomachinery blade rows. In this respect, the thermodynamic aspects of phase-change can be completely divorced from fluid dynamical considerations so that the use of the "black-box" is effectively independent of any particular Computational Fluid Dynamic application. Thus established single-phase CFD codes can, rather easily, be modified to deal with non-equilibrium two-phase flow with the above-mentioned modular approach. (The flexibility of this scheme may be appreciated from Ref. 8 where the same "black-box" has been grafted into a streamline curvature calculation procedure.)

The development of the computational routines within the "black-box" represents a comparatively major undertaking and has been fully described by Guha and Young[4] and Guha[2]. The routines are sufficiently general and robust to deal with any type of nucleating or wet steam flow and (in contrast to many procedures reported in the literature) full details of the polydispersed droplet size spectrum following nucleation are retained in the calculations. The last aspect is essential for accurate modelling of the nucleation zone. This has been possible, without consuming excessive CPU time, by developing a novel averaging procedure that constantly redefines the average size and droplet number in each droplet group. In this way, the number of droplet groups required is restricted to an affordable optimum, while always retaining the correct shape of the droplet size spectrum.

A mixed Eulerian-Lagrangian technique is used. The continuity and momentum equations are solved by Denton's time-marching method. (The wet-steam "black-box" being flexible and modular, any other Eulerian time-marching method, e.g. Jameson's scheme, can be used.) The "black-box" performs the integration of the droplet growth equations along the fluid path lines rather than the usual, quasi-unsteady, method in which the pressure field remains frozen at a given instant of time while the growth of the liquid phase is calculated. The present scheme allows simultaneous solution of all the relevant equations and enforces the correct coupling between the

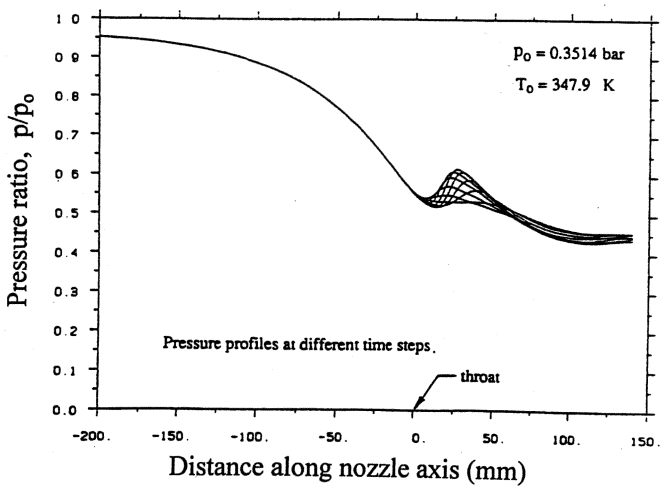

Figure 1. Unsteady condensation: evolution of pressure for one cycle.

vapour-phase gasdynamics and the relaxation effects due to the presence of the liquid phase.

For a proper comparison between experiments and theory, variation in pressure as well as droplet size must be considered. Many references compare the variation in pressure only. Such comparison is an inadequate test for nucleation and droplet growth theories. Almost any nucleation theory can be "tuned" to reproduce the measured pressure distribution. A crucial test is to find out whether the same "tuning" can predict the correct droplet size as well. Experience with calculations for wet steam points out categorically that, in general, predicting a satisfactory pressure distribution does not automatically ensure a good prediction of droplet size. The present computational scheme has been validated against measurements of steady (both sub and supercritical) and unsteady condensation shock waves[4]. Various regimes of condensation have been computed by Guha[2], which shows a novel example of subsonic condensation where the nozzle is unchoked at the geometric throat. (In most reported studies on condensation shocks in nozzles, condensation takes place in the supersonic divergent part.)

Figure 1 presents one example of unsteady calculation. The prediction compares well with measurement. The pressure profiles at different instants during a complete cycle reveal exactly the same sequence of the formation and movement of the shock wave as explained earlier. As the aerodynamic shock wave moves upstream towards the throat and interacts with the nucleation zone, progressively fewer droplets are nucleated thus resulting in a larger final mean radius. This causes a large variation in the droplet size during each cycle. An interesting implication of the unsteady nucleation process is that it may be a contributing factor to the formation of the highly-skewed polydispersed droplet spectrum measured in a real steam turbine: a polydispersity which cannot be predicted with steady flow calculation methods (see Section 4). Details of this and other calculations are in references[2, 4].

2.3 Integral analysis: condensation wave theory

A great deal of physics may be learnt from an integral analysis, which is a study of the jump conditions relating the end states of the condensation zone, without considering the detailed flow structure within it. Reference 2 presents condensation wave theory in great detail and discusses similarities and differences with the more familiar combustion wave theory. A theory of thermal choking is presented in Ref. 3.

3.0 FLUID DYNAMICS WITH INTERPHASE TRANSPORT OF MASS, MOMENTUM AND ENERGY IN PURE VAPOUR–DROPLET MIXTURES

3.1 Relaxation gas dynamics for vapour–droplet mixtures

A lucid description covering many aspects of relaxation gas dynamics and its applications to vapour–droplet flows (including coupled relaxation processes) may be found in[1].

A direct result of the relaxation processes is that various sound speeds may be defined subject to different mechanical and thermodynamic constraints, the two limiting cases being the frozen and the full equilibrium speed of sound. The frozen speed corresponds to the situation when there is no interphase transfer of mass, momentum or energy. The full equilibrium speed results when the two phases remain in equilibrium at all times. Depending on the upstream velocity and mass fraction of the dispersed phase, many different types of shock wave structures may result[1, 2, 5, 6] — e.g. a fully dispersed wave or a partly dispersed wave. A partly dispersed wave consists of a near-discontinuous wavefront, called the frozen shock which is similar to an aerodynamic shock wave in a single-phase gas, followed by a relaxation zone. In a fully dispersed wave flow properties change continuously between the upstream and downstream ends.

Here, we present numerical solutions for a shock wave moving through a vapour–droplet mixture. From a computational fluid dynamics point of view it is quite a formidable task as it involves modelling the effects of interphase transport of mass, momentum and energy on top of the usual complications in predicting moving shock waves in a single phase, ideal gas. In contrast to the calculation of condensation waves described in Section 2, here the slip between the velocities of the two phases are to be accounted for. A mixed Eulerian-Lagrangian technique has been employed[7]. The two-phase continuity, momentum and energy equations are solved by a finite volume, time-marching method. The interphase transfer processes are, however, more easily describable in a Lagrangian framework. They are therefore integrated along the droplet pathlines and are coupled to the unsteady Euler solver by introducing their effects as source terms in the continuity, momentum and energy equations.

3.2 Computational fluid dynamics applied to prediction of moving shock waves in vapour–droplet mixtures

The physical significance of the various wave profiles mentioned above can be appreciated more readily by considering their development under unsteady flow conditions. As a typical example, we now discuss wave generation in one-dimensional flow by an instantaneously accelerated piston in a frictionless pipe initially containing stationary wet steam. The numerical scheme and other details may be found in[7].

Figure 2 shows the numerical prediction of a wave propagating in wet steam. The figure also includes the flow behaviour in a dry, perfect gas under identical conditions in order to illustrate the special features of a vapour–droplet mixture. The perfect gas case is also calculated to verify the accuracy of the numerical scheme by comparing the results with known analytical solutions.

Theory predicts that a shock wave of constant strength propagates at constant velocity into the stationary perfect gas. The gas velocity behind the wave is constant and equal to the speed of the piston. The numerical solution for the pressure distribution, shown by the dotted line in Fig. 2, shows that the computed shock profile and wave velocity are extremely accurate and remain remarkably constant as the wave propagates along the pipe.

When the fluid is wet steam, instead of a perfect gas, the flow physics (as well as the numeric) becomes more complicated. The

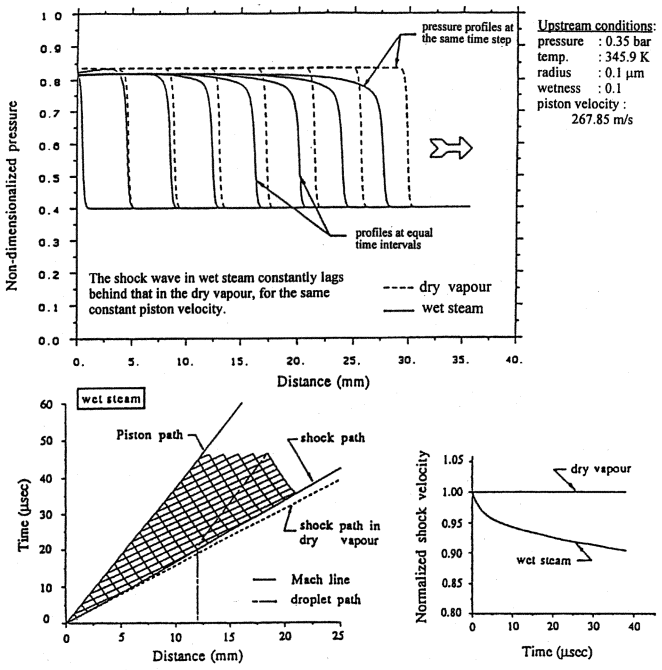

Figure 2. Numerical prediction of shock propagation in a pipe.

$(t - x)$ diagram in Fig. 2 was constructed from the results of the unsteady time-marching calculation. At the instant of initiation, all the interphase transfer processes are frozen and the shock velocity corresponds to the propagation velocity into a single-phase vapour at the same temperature. Behind the shock, the mixture relaxes to equilibrium along the particle pathlines, a typical example of which is shown in the $(t - x)$ diagram. The droplet temperature relaxes first on the very short timescale τ_D and is followed by the velocity slip and vapour temperature on timescales τ_l and τ_T respectively. Changes along the particle paths are propagated upstream and downstream along the left and right running Mach lines (based on the frozen speed of sound). The right running Mach lines overtake the shock wave, weakening it and causing it to slow down. The shock path therefore curves in the $(t - x)$ diagram until it reaches a constant equilibrium speed. When this occurs, the dispersive effects of the relaxation processes are just balanced by the steepening effects of the non-linear terms and the wave structure is identical to that of the stationary waves in steady flow described earlier. Whether the final equilibrium structure is partly or fully dispersed depends on the piston velocity (for analytical conditions, see Ref. 1).

The variation of the wave pressure profile with time is also shown in Fig. 2 and the deceleration and weakening of the wave front are clearly visible. The behaviour of the superheat vapour temperature, droplet radius and wetness fraction is shown by the curves in Fig. 3 which are self-explanatory. As with stationary partly dispersed shock waves, the increase in wetness fraction downstream of the frozen shock wave is due to the effects of velocity slip.

3.3 Integral analysis: jump conditions

Detailed study on the jump conditions across shock waves has been made[2, 5] and the similarities and differences of condensation discontinuities and aerodynamic shock waves are discussed at length in Ref. 2. The integral analysis reveals that, depending on the upstream wetness fraction and the pressure ratio across the wave, four types of shock structures may result in vapour–droplet flow. They are: (*i*) equilibrium fully dispersed, (*ii*) equilibrium partly dispersed, (*iii*) fully dispersed with complete evaporation, (*iv*) partly dispersed with complete evaporation. Jump conditions or Rankine-Hugoniot relations appropriate for each case are derived[2, 5] and the mechanism of entropy production have been discussed[5].

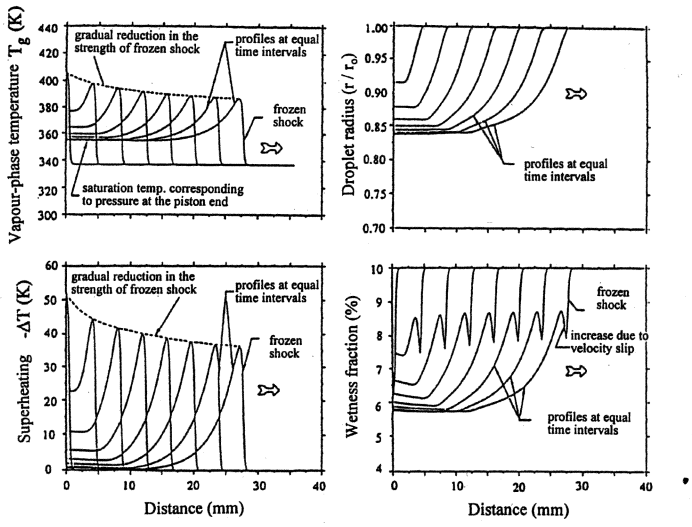

Figure 3. Variation of flow parameters during shock propagation in wet steam.

4.0 APPLICATION OF THE NON-EQUILIBRIUM THEORY TO STEAM TURBINES

4.1 The formation of the liquid phase

An introduction to the flow through steam turbines may be found in Ref. 1. In a multistage steam turbine used in power plants for generating electricity, the steam enters the low-pressure (LP) turbine cylinders as a dry superheated vapour but becomes wet towards the last stages. Experiments show that the water in turbines exists in two quite different forms. Usually more than 90% of the mass is concentrated in the fog, which consists of very large number of very fine droplets (diameter 0·05-2·0 μm). The rest is in the form of coarse droplets which are very much larger (diameter 20-200 μm). Coarse water is formed as a small proportion of the fog (typically 2-3% per blade row) is deposited on the blade surface either due to inertial impaction or through turbulent diffusion. The deposited water is drawn towards the trailing edge by the steam flow (or centrifuged towards the casing on moving blades), where it is re-entrained in the form of large droplets. The large droplets cause blade erosion, but their thermodynamic and mechanical effects on the steam flow can nearly always be neglected.

Formation of new droplets occurs only over a small part of the expansion in a turbine. As a fluid particle flows through the machine, typically the complete nucleation process takes only 10-20 μs, as compared with a typical flow transit time of 5-10 ms through an LP turbine. Thus most of the expansion in the turbine simply involves condensation on existing droplets. However, nucleation is of crucial importance as it is the process which establishes the final fog droplet size distribution which, in turn, determines the subsequent departure from equilibrium affecting the flow behaviour, the magnitude of the wetness loss and the rate of fog droplet deposition on the blading forming coarse water. Once the droplet size distribution can be accurately predicted, the analysis of the wet steam flow through the rest of the turbine rests on more solid foundation. However, currently no theory exists (see Section 4.2 for a novel theory) which gives even remote agreement with the available experimental measurements of the size distribution of fog droplets in turbines.

Our inability to understand the nucleation process in steam turbines is surprising given the success with which spontaneous condensation in laboratory nozzles and stationary, two-dimensional, laboratory cascade of steam turbine blades can be predicted using a synthesis of the classical theories of homogeneous nucleation and

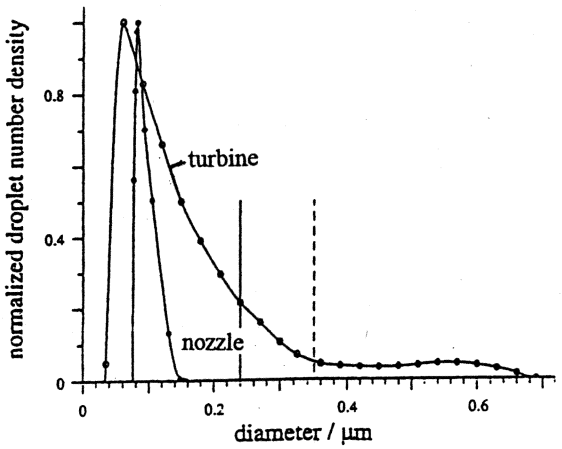

Figure 4. Typical droplet size distributions in a supersonic condensing steam nozzle (computed) and in the exhaust of a low pressure, electricity generating steam turbine (inferred from optical transmission data). ------ Sauter mean, ——— mass mean. Turbine measurements courtesy of P.T. Walters, National Power Technology and Environment Centre, Leatherhead, UK.

droplet growth with the conservation equations of gas dynamics. Such calculations have now been refined to the extent that the theory, amended by only a modicum of empiricism, gives acceptable agreement in terms of pressure distribution and mean droplet diameter with most experiments reported in the literature.

As shown in Fig. 4, calculations of droplet size spectra in condensing steam nozzles usually indicate a narrow distribution with a comparatively small mean droplet diameter strongly dependent on the local expansion rate near the Wilson point. The mean droplet size is sensitive to inlet conditions, small changes of which can displace the Wilson point to new locations of quite different expansion rate. In turbines, however, experimental determinations of droplet size spectra give quite different results, the optical characteristics of the medium invariably indicating a broad, strongly skewed, distribution with a much larger mean diameter, typically in the range 0·2-0·6 μm. Quite often, the distribution is bimodal with a significant proportion of the total mass of liquid contained in a secondary population of droplets having diameters in the range 0·4-1·0 μm. Furthermore, the spectrum is comparatively insensitive to small changes in turbine inlet conditions and measurements taken on the same machine over a period of years show excellent reproducibility.

It is therefore evident that the nucleation of water droplets in turbines involves phenomena which are not reproduced by laboratory experiments on nozzles and stationary cascades, but nevertheless play

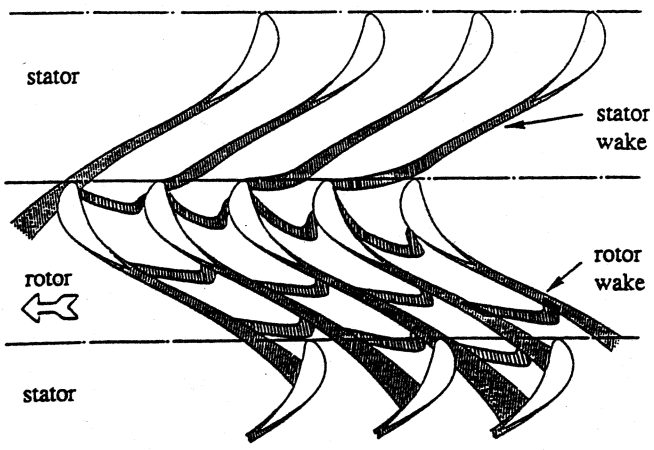

Figure 5. Schematic diagram of the passage of blade wakes through successive blade rows.

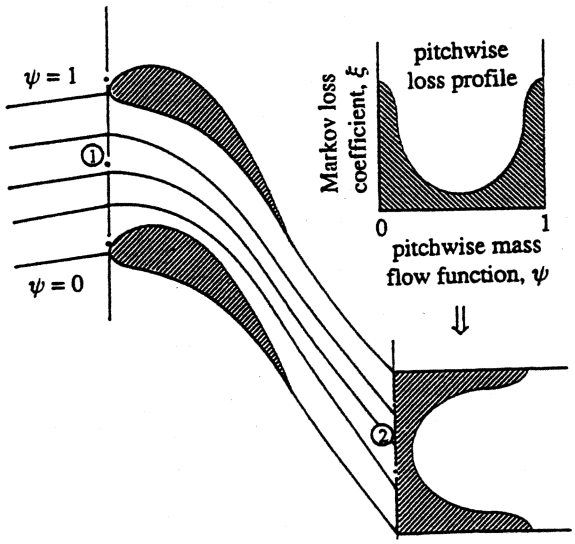

Figure 6. Specification of the pitchwise loss profile for a blade row.

a dominating role in the process of phase-transition in real machines. Possible explanations include nucleation in blade-wake vortices, heterogeneous condensation due to the effects of impurities in the steam and the effects of blade-row interaction unsteadiness. In Section 4.2, consideration is given to the third of these possibilities.

4.2 A new theory of nucleation of water droplets in multi-stage steam turbines used in power plants

The details of the theory are given Refs 1 and 8. The essence of the theory is that large-scale temperature fluctuations caused by the segmentation of blade wakes by successive blade rows have a dominating influence on nucleation and droplet growth in turbines. The fundamental premise is that, in passing through a multi-stage turbine, different fluid particles undergo different fluid mechanical experiences depending on the exact details of their passage through the machine and hence arrive at a given axial location with a wide variety of thermodynamic conditions. It is further assumed that, downstream of any turbine stage, the pressure of all the fluid particles would be near-uniform but their specific entropies (and hence static temperatures) would vary greatly depending on the dissipation experienced by a particular particle due to its being entrained in one or more blade boundary layers or loss-generating regions of the flow. However, although the path taken by a fluid particle is assumed to be random, the time-averaged dissipation of all the particles should agree with the overall loss distribution in the turbine. This is assumed to be known, either by direct measurement or from empirical loss correlations.

Figure 5 is a schematic diagram of the way in which the wakes from one blade row interact with, and are segmented by, the following row. It can be clearly seen that dissipation occurring in successive blade rows can become superposed in certain fluid particles (the darkly shaded areas).

A Lagrangian frame of reference is adopted and attention is focussed on a large number of individual fluid particles during their passage through the turbine. Homogeneous nucleation and growth of droplets in each fluid particle is assumed to be governed by classical theories. All fluid particles are assumed to experience the same pressure variation but those particles passing close to the blade surfaces suffer greater entropy production and therefore have higher static temperatures than those which pursue near-isentropic paths through the central portions of the blade passages. Particles which suffer high loss therefore nucleate later in the turbine than those which experience little dissipation. Condensation is thus viewed as an essentially random and unsteady phenomenon as the dissipation experienced by a fluid particle in one blade-row is assumed to be uncorrelated with

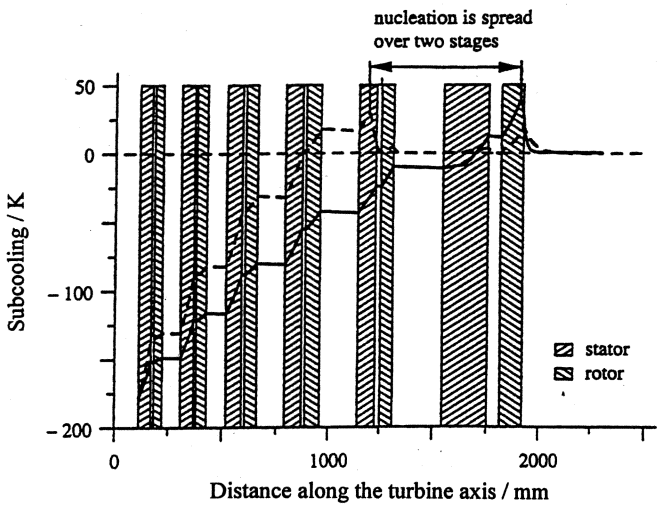

Figure 7. Axial variation in the Ansaldo turbine of vapour subcooling for two fluid particles representing the extreme cases of zero dissipation (-----) and maximum dissipation (——).

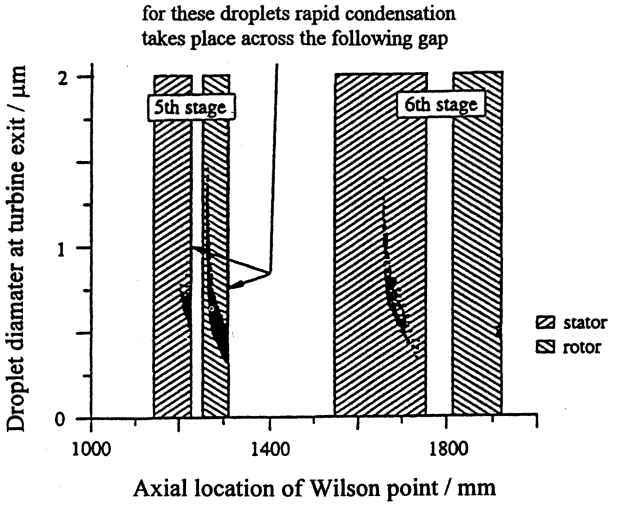

Figure 8. Computed Sauter mean droplet diameter at Ansaldo turbine outlet as a function of the axial location of the Wilson point for all fluid particles.

its previous history. On a time-averaged basis, the condensation zone is spread over a much greater distance in the flow direction than a simple steady-flow analysis would indicate and may encompass several blade-rows depending on the number of stages in the machine.

As shown in Fig. 6, a "loss profile" is constructed to represent the pitchwise distribution (from the suction to the pressure surface) of the loss in the blade-row. The pitchwise loss profiles represent the time-averaged entropy increase along particular pathlines but individual fluid particles associated with the passage of wakes may exit from the blade-row at different conditions because, on entry, their static temperatures and velocities deviate from the mean.

For the results presented below, a single (circumferentially averaged) pressure-time variation based on an axisymmetric streamline-curvature throughflow solution was adopted for all fluid particles. Fluid particles are then launched at the turbine inlet (where the steam is superheated), all at the same stagnation temperature and pressure. At the entry to each blade row a random number is generated that specifies the pathline to be followed by the particle. The pathline, in turn, fixes the value of the polytropic efficiency (Fig. 6). The "black-box" (Section 2.2) is then applied along the pathline to calculate the subcooling and the droplet size distribution (if nucleation has taken place) at the downstream of the particular blade row. A new random number is then generated that specifies the pathline in the next blade row and the procedure is repeated. The "black-box" can deal with successive nucleations after the primary as a matter of course should the expansion be sufficiently rapid to generate the high levels of subcooling required.

For each fluid particle, the subcooling and droplet size distribution at all points of interest are recorded. It is then a straightforward matter to compute the time-mean wetness fraction and other statistical properties in order to obtain a quantitative picture of the process of phase-change and liquid growth throughout the machine. In a six-stage low-pressure turbine, some 10^4 fluid particle calculations are undertaken on each streamsurface to obtain converged statistical properties.

As an example of the Monte Carlo simulation, the flow through the low pressure stages of a 320 MW turbine was analysed. The turbine was manufactured by the Italian company Ansaldo and the complete geometry is available in the literature[1, 8]. The LP section has six-stages. Each stage consists of a stator followed by a rotor and hence there are twelve blade-rows altogether in the turbine.

The physical characteristics are best explained by adopting a Lagrangian viewpoint of a fluid particle as it passes through the turbine. As described in the previous sections, different fluid particles experience different amounts of dissipation and heat transfer, depending on the particular pathline followed. Two limiting cases can be identified. At one extreme are the fluid particles which always follow the mid-pitch pathline in each blade-row and consequently suffer no dissipation. They pursue an isentropic path to the Wilson point. At the other extreme are those particles which negotiate the regions of maximum loss in each blade-row. Other fluid particles experience levels of loss intermediate between these two extremes.

Figure 7 shows the calculated variation of the vapour subcooling ΔT associated with the two extreme cases of zero and maximum dissipation. The subcooling of the fluid particles change as a result of the competing effects of the three physical processes: expansion, condensation and dissipation. Consider first the case of the fluid particle suffering no dissipation. Here, one of the mechanisms for altering the subcooling, i.e. dissipation, is absent. The fluid particle is superheated (negative ΔT) at the turbine inlet. Its subcooling increases in each blade-row due to expansion but remains almost constant between the rows. It attains the Wilson point in the stator of the fifth stage and subsequently experiences an exponential decrease in ΔT due to the extremely rapid liberation of latent heat. ΔT increases significantly again in the last rotor where the expansion rate is too high to be offset by the counteracting effect of condensation. Much the same history is repeated for the fluid particle experiencing the maximum dissipation. Here, however, dissipation opposes the increase of the subcooling throughout the flowfield. Consequently, the Wilson point occurs much further downstream (in the rotor of the last stage). Other fluid particles, experiencing intermediate amounts of dissipation, attain their Wilson Points at intermediate locations between the two extremes. The region of nucleation thus covers (in a randomly unsteady manner) almost two complete turbine stages as opposed to being restricted to a very narrow zone in a specific blade-row.

A reliable "rule of thumb" is that Wilson points occurring at locations of higher expansion rate result in smaller droplets. The variable location of the Wilson point therefore results in large variations in mean droplet diameter. It should be understood, however, that the mean droplet diameters in the two limiting cases do not necessarily represent the extreme limits of droplet size produced in the machine. The droplet size is dependent on the local expansion rate which does not vary monotonically with distance between the extreme locations of the Wilson points.

Figure 8 shows the location of the Wilson points for the totality of particles considered (10^4). Each point on this diagram corresponds to an individual fluid particle. The abscissa denotes the axial location of the Wilson point and the ordinate denotes the mean diameter of droplets within the fluid particle on its arrival at the turbine outlet. It

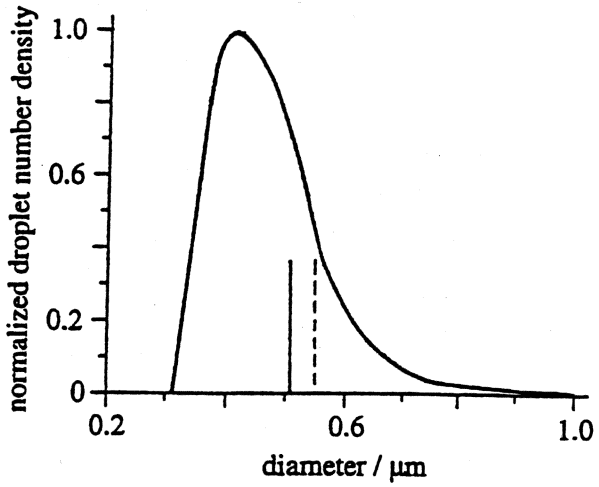

Figure 9. Computed time-averaged droplet size distribution at outlet of the Ansaldo turbine. —— mass mean, ----- Sauter mean.

can be seen that the majority of fluid particles nucleate either in the fifth-stage rotor or in the sixth-stage stator. (The absence of Wilson points in the first part of the sixth-stage stator results from the very low expansion rate there, see Refs 1 and 8.) In each blade-row, the mean diameter of the droplets becomes progressively smaller as the Wilson point moves towards the trailing-edge, as the rate of expansion tends to increase monotonically to each blade throat. However, interesting behaviour results for those fluid particles that reach the trailing-edge plane with subcoolings and nucleation rates which, although moderately high, are still insufficient to cause complete reversion to equilibrium. For these particles, the trailing-edge marks the Wilson point (i.e. the cessation of nucleation) even if comparatively few droplets have yet been produced. Reversion to equilibrium then occurs within the following gap by condensational growth on existing droplets. Because there is plenty of time available and because the droplet number density is low, these droplets may grow to very large sizes as shown in Fig. 8. Such fluid particles are then prime candidates for secondary nucleations in succeeding blade-rows because their liquid surface area is insufficient to offset (by condensation) the opposing effect of increased subcooling due to the rapid expansion.

An imaginary probe with unlimited resolution in space and time, sited at the turbine outlet, would register the complete droplet size distribution for each fluid particle it encounters. Real probes based on the measurement of attenuated or scattered light, however, record only sufficient information to deduce, at most, the time-averaged droplet size distribution (and sometimes only the time-averaged Sauter mean diameter). In order to compare the theoretical predictions with such measurements, a theoretical time-averaged droplet size distribution may be constructed at any axial location in the turbine, if the diameters and number density of droplets in all the 10^4 fluid particles considered are recorded by the computer for subsequent processing. The calculated time-averaged droplet size distribution for the Ansaldo turbine at outlet is shown in Fig. 9. The spectrum is polydispersed and highly-skewed (i.e. there is a large difference between the mean and most probable diameters) and resembles the shape of similar spectra measured in real turbines (Fig. 4). This is very significant, as no existing steady-flow calculation procedure can predict such a high degree of polydispersion.

Unfortunately, no measurement of the droplet size distribution is available for the Ansaldo turbine, although the time-averaged Sauter mean diameter of the droplets has been measured. The measured Sauter mean diameter at mid-span is about 0·4 μm, which is a little smaller than the calculated value of 0·55 μm, shown in Fig. 9. However, allowing for the uncertainties and approximations in the calculation scheme, the level of agreement is extremely encouraging. Of course, many more experimental comparisons are required before it is possible to assert conclusively that the important physical processes are being successfully modelled by the theory presented.

4.3 Conclusion

A theory has been developed for predicting the effect of temperature fluctuations on the homogeneous nucleation and growth of water droplets in multi-stage steam turbines. The fluctuations result from the segmentation of blade-wakes by successive blade-rows and the amplitude of the fluctuations increases with the number of stages. According to the model, the mechanics of nucleation in multi-stage turbines are quite different from the predictions of conventional steady-state theories of phase-change. For example, the nucleation zone may encompass (in a randomly unsteady manner) several blade-rows (as opposed to being isolated at a particular position in a specific blade-row). The inherent unsteadiness of the process also results in a highly-skewed, polydispersed (sometimes bimodal) time-averaged droplet size distribution, having similar characteristics to spectra measured in real turbines. The next step would be to include, in the calculation scheme, the effects of circumferential variation in pressure within the blade passages.

The fundamental implication of the theory is that the time-average of the droplet spectrum that results from nucleation and droplet growth in a fluctuating flowfield (due to wake segmentation in a multistage machine) is quite different from the droplet spectrum that is calculated by first determining a time-average flowfield and then performing nucleation and droplet growth computations in this steady field. The theory presents a radically different perspective of nucleation in turbines from the generally accepted view and, if correct, should have a major influence on the future development of calculation procedures for non-equilibrium steam flows in turbines.

5.0 A UNIFIED THEORY FOR THE INTERPRETATION OF TOTAL PRESSURE AND TEMPERATURE IN VAPOUR–DROPLET OR GAS-PARTICLE TWO-PHASE FLOW

In this section we discuss briefly some interesting effects of the non-equilibrium, interphase transfer mechanisms in a stagnation process in two-phase flow[9]. Pitot measurements are often used for inferring velocity or loss (entropy generation) in multiphase mixtures. In single phase fluids, the fluid is assumed to be brought to rest at the mouth of the Pitot tube isentropically. Hence flow Mach number and entropy generation (in steady, adiabatic flow) are uniquely determined by the total pressure measured by a Pitot tube, together with an independent measurement of the static pressure. (In supersonic flow in an ideal gas, application of Rankine-Hugoniot equations across the detached shock wave in front of a Pitot tube retains the utility of Pitot measurements for deducing flow Mach number and entropy generation.) The measurement and interpretation of total pressure as well as of total temperature in a multiphase mixture require careful considerations[9].

The solid particles or the liquid droplets respond to changes in temperature, velocity, etc. of the gas phase through interphase exchanges of mass, momentum and energy. These are essentially rate processes and hence significant departures from equilibrium can take place if the rate of change of external conditions, imposed by the deceleration in the stagnating flow, is comparable to the internal time scales. Thus, for example, if the size of the liquid droplets or the solid particles is very small, then inertial and thermodynamic equilibrium between the two phases are always maintained, and a Pitot tube would measure the equilibrium total pressure, p_{0e}. On the

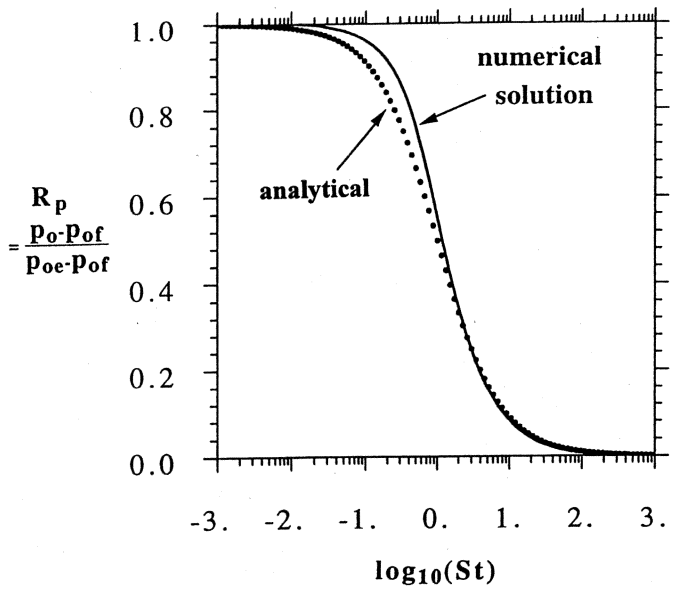

Figure 10. Near-universal plot of R_p *versus* S_t; comparison of a simple analytical theory with numerical solutions.

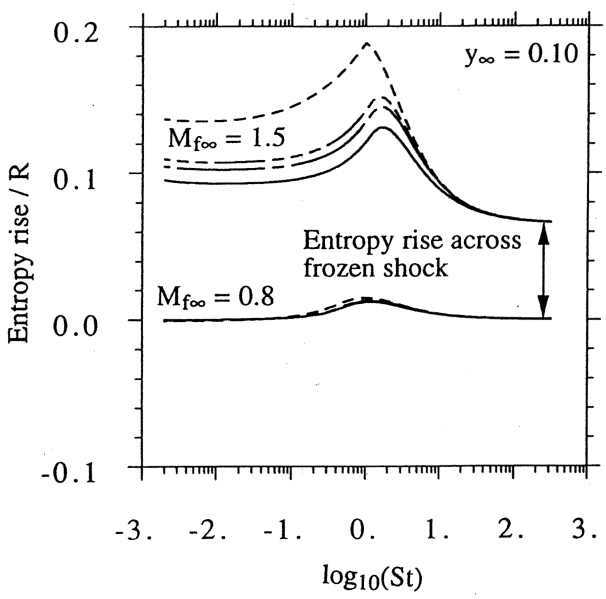

Figure 11. Entropy rise *versus* Stokes number in air with different solid particles. (—— $\delta = 0{\cdot}1$, - — - $\delta = 0{\cdot}8$, - - - — $\delta = 1{\cdot}2$, - - - - $\delta = 4{\cdot}0$).

other hand, if the size of the droplets or the particles is very large, all interphase transfer processes remain essentially frozen. The Pitot tube records the pressure which it would have recorded if the vapour phase alone was brought to rest from the same velocity. The total pressure in this case is termed the frozen total pressure, p_{0f}. Analytical expressions for p_{0e} and p_{0f}, both in vapour–droplet and gas-particle flow, are given in[9].

As an example, consider low-pressure wet steam with a typical wetness fraction of 10% and at a Mach number 1·5. Calculations show that $p_{0f}/p = 3{\cdot}3$ and $p_{0e}/p = 3{\cdot}79$, where p is the static pressure. Therefore, in this particular example, the equilibrium total pressure is about 15% higher than the frozen value.

It is expected that for intermediate sizes of the droplets or particles, the pressure recorded by the probe would neither be the equilibrium nor the frozen value. The imposed deceleration in front of the Pitot tube would cause the two-phase mixture to deviate from equilibrium conditions, both inertially and thermodynamically. The deceleration process consequently ceases to be isentropic, as non-equilibrium exchanges of mass, momentum and energy between the two phases create entropy.

Guha has considered[9] a large number of two-phase mixtures, both gas-particle and vapour–droplet, at subsonic as well as supersonic velocities for many different sizes of the droplets (or particles). In the supersonic case a detached frozen shock wave stands in front of the Pitot tube. The relaxation mechanisms in a gas-particle mixture are different from those in a vapour–droplet flow. Despite all these complexities and differences, it was possible with proper non-dimensionalisation of flow parameters to adopt a universal plot, within acceptable tolerance, of non-dimensional total pressure, R_p, *versus* Stokes number, S_t (which is a non-dimensional representation of particle size). R_p and S_t are defined by, $R_p = (p_0 - p_{0f})/(p_{0e} - p_{0f})$ and $S_t = \tau_l V_\infty/L$, where, V_∞ is the unperturbed velocity of the two-phase mixture far upstream of the measuring device, p_0 is the pressure attained at the measuring point under non-equilibrium conditions (the total pressure which is measured) and L is a characteristic length (in subsonic flow L is related to the Pitot diameter, in supersonic flow L is related to the distance between the frozen shock wave and the Pitot mouth). Larger droplets or particles correspond to higher S_t.

Figure 10 shows the variation of R_p with S_t, which may be adopted as the Pitot correction curve usable at a wide range of subsonic and supersonic Mach numbers and for any two-phase mixtures (vapour–droplet or gas-particle). The variation is monotonic. It should be noted that the denominator in the expression for R_p is calculated using the equilibrium thermodynamics, whereas the numerator is calculated using non-equilibrium equations. That the value of R_p, shown in Fig. 10, indeed tends to unity and zero in the appropriate limits of S_t, demonstrates independent theoretical consistency of the calculation schemes.

In addition to these numerical calculations, an analytical theory for determining total pressure under non-equilibrium conditions has been formulated (as yet unpublished). The analytical theory is simple and is amenable to direct physical interpretation. The theory shows that $R_p = 1/(1 + S_t)$. The predicted total pressure correctly reduces to the frozen total pressure in the limit of large Stokes number (large particles) and to the equilibrium total pressure in the limit of small Stokes number (small particles). Maximum dependence of the total pressure on Stokes number is observed when the Stokes number is of the order unity. The analytical result is also plotted in Fig. 10 for comparison. Under non-equilibrium conditions for intermediate S_t, the prediction of this equation compares very well with results from full numerical solution of the gas dynamic equations for two-phase mixtures.

Figure 11 plots the rise in mixture entropy, as mixtures of air and solid particles are decelerated by a measuring probe from their far upstream velocity to rest. Four different (hypothetical) solid particles with $\delta \equiv c_l/c_{pg} = 0{\cdot}1$, $0{\cdot}8$, $1{\cdot}2$ and 4 are considered (where δ is the ratio of specific heats of the solid and the gas) and the calculations are performed for two upstream frozen Mach numbers ($M_{f\infty}$). For the subsonic case ($M_{f\infty} = 0{\cdot}8$), Fig. 11 shows that the rise in entropy is indeed maximum when $S_t \sim 1$, and is almost zero in the frozen and equilibrium limits. (Recall from Fig. 10 that the total pressures are different in these limits.) At $M_{f\infty} = 1{\cdot}5$, the entropy rise is again maximum close to $S_t \sim 1$, but it has a finite value both at $S_t \to 0$ and at $S_t \to \infty$. The rise in entropy in the limit $S_t \to \infty$ is simply that across the frozen shock. (Since the same frozen shock is involved in all cases because the same $M_{f\infty}$ is used, this increase in entropy is the same for all four mixtures considered.) The rise in entropy in the limit $S_t \to 0$ is, however, different for different mixtures (it depends on the isentropic index of the mixture and hence on δ). However, it is shown[5] that if the particles come to equilibrium downstream of a frozen shock wave, then the entropy rise (across the shock plus the relaxation zone) is not dependent on the particle size (and hence on the relaxation times), but is determined completely by Rankine-Hugoniot equations for two-phase flow. This fact is reflected in the straight, horizontal portions of the curves (at $M_{f\infty} = 1{\cdot}5$) in Fig. 11 in the limit $S_t \to 0$.

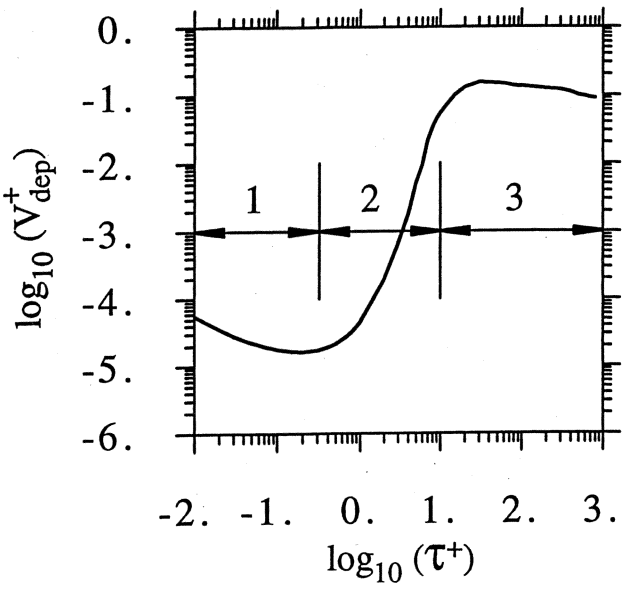

Figure 12. A typical variation in measured deposition rate with particle relaxation time. Zone 1: turbulent diffusion regime, zone 2: turbulent diffusion — eddy impaction regime and zone 3: particle inertia moderated regime.

The rate of entropy production in a multiphase mixture is maximum when the Stokes number is of the order unity (in accordance with other results of relaxation gas dynamics), and a reduction in measured total pressure is not unequivocally related to a rise in entropy (as it is in steady, adiabatic flow of single-phase fluids). The fact that the total pressure decreases monotonically from p_{0e} to p_{0f} as S_t changes from 0 to ∞ (Fig. 10), whereas the entropy rise is zero at both limits and has a maxima when $S_t \sim 1$ (Fig. 11), demands care while interpreting Pitot measurements in multiphase flow.

6.0 A UNIFIED EULERIAN THEORY OF TURBULENT DEPOSITION TO SMOOTH AND ROUGH SURFACES

6.1 Introduction

Understanding the mechanisms by which particles dispersed in a turbulent stream of fluid are transported towards the solid walls forming the flow passage, and predicting the rate of deposition, are both scientifically interesting and of engineering importance (in a variety of areas of mechanical engineering, chemical engineering, environmental engineering and physiology). Consequently these have been the subject-matter of an extremely large number of studies.

Guha[10] has developed, a simple, unified Eulerian theory of deposition that can be used for practical calculations. Starting from the fundamental conservation equations and with a modicum of approximations and no tuning factors, the present theory produces satisfactory agreement with the experimental data. (Typical experimental data is schematically shown in Fig. 12, which is a plot of non-dimensional deposition velocity versus non-dimensional relaxation time; $\tau^+ = \tau_l u^{*2}/\nu$, where τ_l is the inertial relaxation time of the particles, u^* is the fluid friction velocity and ν is the kinematic viscosity of the fluid. $V^+_{dep} = J/\bar{\rho}_{p_0} u^*$, where J is the mass flux of particles and $\bar{\rho}_{p_0}$ is the bulk partial density of particles.)

There are two common approaches for deposition calculations: Eulerian and Lagrangian. On the Eulerian front, the established practice has been to use separate theories for capturing the different behaviours of deposition rate in different size ranges of particles. With reference to Fig. 12, a turbulent version of Fick's law is applicable for the small particles, "free flight" or "stopping distance" models are for the intermediate range, and yet another model is to be applied for large particles. Although it is possible, with proper tuning of the models (e.g. by prescribing the free flight velocity), to reproduce the experimental results for fully developed pipe flow, the theories cannot be extrapolated to two or three dimensional flow situations (e.g. for deposition of particles on gas turbine blades) with any great confidence because of their piecemeal nature and the required empirical tuning. These models are also of limited use if other effects, e.g. thermophoresis or electrostatic interaction, are present.

The Lagrangian scheme, on the other hand, involves trajectory calculations typical for a large number of particles, the fluid turbulence field being generated by various methods ranging from simple to direct numerical simulation (DNS) of Navier-Stokes equations. These calculations are illustrative and important for physical understanding. However, Lagrangian computations may be too time-consuming to be effective as a practical calculation method, especially for small particles. Many reported Lagrangian schemes also do not reproduce the whole deposition curve as shown in Fig. 12.

The present theory is Eulerian in nature but results in a universal set of simple equations that apply for the whole size range of particles and explain the physics of the problem to a great extent. The present scheme has the potential of becoming a useful tool in practical calculations of any complexity as well as theoretical analyses of fundamental importance.

The present theory of deposition is general. Other than Fickian diffusion (both Brownian and turbulent), the theory includes motion of particles due to temperature gradient (thermophoresis), motion arising from interaction of particle inertia with the inhomogeneity of turbulence field (turbophoresis), motion of particles due to electrical forces (electrophoresis), motion due to gravity and Saffman lift force, and the effects of surface roughness. It is possible to extend the theory to include other effects such as pressure diffusion, stressphoresis or diffusiophoresis.

The theory is mathematically quite sound and should be useful in understanding the physics of deposition process. However, one of the main strength of the theory is its simplicity and practical relevance. It is shown[10] that the solution of a simple set of equations, the continuity Equation (1) and two momentum Equations (2a) and (2b), produce the whole of the "S-shaped" deposition curve and give results which compare favourably with the most advanced and elaborate Lagranginan-type particle tracking methods. (In fact, it is shown that the solution of just one momentum Equation (2c) could be enough in many cases, the compromise being the neglect of the Saffman lift force.)

The present scheme, being Eulerian, is computationally much faster than stochastic Lagrangian calculations of particle tracking (by several order of magnitude in the case of small particles). It is also more versatile than any other reported calculation scheme (in its applicability to the whole size range of particles and its ability to account for various deposition mechanisms). Since the present theory models the various deposition mechanisms correctly, it should be applicable to practical deposition problems in complex geometries (e.g. deposition of particles on internally cooled, highly curved, gas turbine blades or that of water droplets on steam turbine blades). It is possible to combine the present Eulerian scheme for calculating particle motion with well-established Eulerian flow solvers for calculating the flowfield of the primary fluid. Thus the present theory could be of interest to fluid dynamicists as well as of use to aerosol engineers.

6.2 The present unified model of deposition

The proper way of deriving the equations for deposition is to write the particle continuity and the momentum conservation equations, split the different flow quantities into their respective mean and fluctuating components, and then perform Reynolds averaging. The details may be found in Ref. 10, here we quote the final results.

Consider vertical, fully-developed flow in a pipe with the x-coordinate aligned to the flow direction and the y-coordinate being perpendicular to the solid wall. The expression for the flux of particles J in the y-direction results from the Reynolds-averaging of the particle continuity equation and is given by

$$J = -(D_B + \varepsilon)\frac{\partial \bar{\rho}_p}{\partial y} - \bar{\rho}_p D_T \frac{\partial \ln T}{\partial y} + \bar{\rho}_p \bar{V}_{py}^c \quad \ldots (1)$$

where D_T is the coefficient of temperature-gradient-dependent diffusion including the thermophoretic component, D_B is the Brownian diffusion coefficient, ε is the eddy momentum diffusivity, $\bar{\rho}_p$ is the average particle concentration, and, T is the temperature. The particle convective velocity in the y direction, $\bar{V}_{py}^c$, appearing in Equation (1), has to be calculated from the particle momentum equation. The particle momentum equations in the y and x directions are given by

$$\bar{V}_{py}^c \frac{\partial \bar{V}_{py}^c}{\partial y} + \frac{\bar{V}_{py}^c}{\tau_I} = -\frac{\partial \overline{V_{py}'^2}}{\partial y} + F_{Sy} + G_{Ey} \quad \ldots (2a)$$

$$\bar{V}_{py}^c \frac{\partial \bar{V}_{px}}{\partial y} = \frac{1}{\tau_I}\left(\bar{V}_{fx} - \bar{V}_{px}\right) + g \quad \ldots (2b)$$

where, $\overline{V_{py}'^2}$ is the square of particle rms velocity, $\bar{V}_p$ is the average particle velocity, $\bar{V}_f$ is the average fluid velocity, F_S is the Saffman lift force, G_E is electrical force, τ_I is the particle relaxation time and g is the acceleration due to gravity. Note that the x-momentum Equation (2b) involves both $\bar{V}_{px}$ and $\bar{V}_{py}^c$. The y-momentum Equation (2a), on the other hand, is almost decoupled and depends on $\bar{V}_{px}$ only through the Saffman Lift force, F_{Sy}. A study of Equations (2a) and (2b) also shows nicely how gravity affects the y-momentum equation through the lift force.

In the general case, both Equations (2a) and (2b) must be solved simultaneously. In order to gain more physical insight into the deposition process, we temporarily suspend the effect of the Saffman Lift force, F_{Sy}, and the electrical force, G_{Ey}. With these provisos, the particle convective velocity in the y direction, $\bar{V}_{py}^c$, can be calculated from

$$\bar{V}_{py}^c \frac{\partial \bar{V}_{py}^c}{\partial y} + \frac{\bar{V}_{py}^c}{\tau_I} = -\frac{\partial \overline{V_{py}'^2}}{\partial y} \quad \ldots (2c)$$

It is worth remembering that the second term in the LHS of Equation (2c) is the steady state drag term simplified with the assumption $\bar{V}_{fy} = 0$; the full form is $-(\bar{V}_{fy} - \bar{V}_{py}^c)/\tau_I$.

The first term in the RHS of Equation (1) is the contribution from Brownian and turbulent diffusion. This term depends on the gradient in the particle concentration and is the same as Fick's law. The second term represents the diffusion due to a gradient in the temperature. The third term represents a convective transport of particles. Equation (2c) relates the particle convective velocity with the gradient in turbulence intensity (turbophoresis). Equation (2a) shows that the lift force and the electrical force also contribute to this convective velocity. It is chiefly the absence of this convective term in Fick's law that necessitated postulating stopping distance models. It is important to note that the turbophoretic term depends on the particle rms velocity, which may be different from the fluid rms velocity if the particle inertia is large. When the particles are very small, they effectively follow the fluid eddies and the two rms velocities are essentially the same. In this limit, $\tau_I \to 0$, Equation (2c) shows that $\bar{V}_{py}^c \to 0$. Hence the contribution from turbophoresis is negligible. Fick's law is, therefore, an adequate description for the deposition of small particles. As τ_I increases, the turbophoretic term assumes dominance, thereby increasing the deposition rate by a few order of magnitude. However, as τ_I increases, the particles are less able to follow fluid fluctuations and the particle rms velocity becomes progressively smaller as compared to the fluid rms velocity. This is one of the factors responsible for the eventual decrease in deposition velocity with

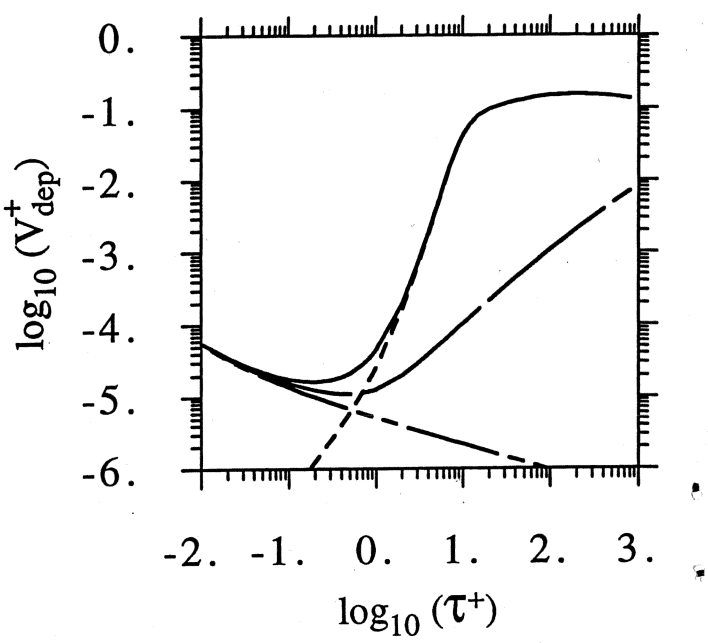

Figure 13. Predicted deposition rate versus relaxation time (effects of pure diffusion, pure inertia and interception).
—— Solution of Equation (1) retaining all terms
- - — Pure diffusion: solution of Fick's law, with the lower boundary at wall ($y_0^+ = 0$)
— — Pure diffusion: solution of Fick's law, with interception ($y_0^+ = r^+$)
- - - - Pure inertial deposition: solution of Equation (1) retaining only the third term on the RHS. For all curves, $k_s^+ = 0$, $\Delta T = 0$.

increasing particle size when τ_I is very large. For small particles the first two terms in the RHS of Equation (1) dominates whereas for large particles it is the third term that matters. That these three distinct mechanisms of deposition appear in a simple additive form in Equation (1) has not been postulated but is rigorously derived from the fundamental conservation equations.

It is crucial to incorporate the particle momentum equation (equation set 2) in the analysis. The first term in Equation (2c) represents particle acceleration, the second term is the viscous drag and the third term arises from the turbulent fluctuations. When $\tau^+ \to \infty$, the viscous drag term is negligible, and the acceleration term is balanced by the turbulence term. However, in this limit, the turbulence term also tends to zero. As τ^+ is decreased from this limit, the turbulence term grows and so does the convective slip velocity $\bar{V}_{py}^c$. The deposition velocity therefore increases with decreasing particle size in this range (Fig. 12, zone 3). This trend in deposition velocity, however, does not continue all the way to very small particles because the viscous drag term assumes importance. The viscous drag term increases with decreasing particle relaxation time, and tries to reduce the slip velocity. The turn over point occurs around $\tau^+ = 30$. For $\tau^+ < 30$, the deposition velocity starts decreasing with decreasing relaxation time (Fig. 12, zone 2). In this regime, the acceleration term loses importance, and the viscous term usually balances the turbulence term. Equation (2c) shows that as $\tau^+ \to 0$, $\bar{V}_{py}^c \to 0$. Turbophoresis is thus negligible for small particles even if there is a gradient in turbulence intensity. However, for small particles the Brownian and turbulent diffusion of particles begin to dominate and the deposition velocity rises again with decreasing τ^+ (Fig. 12, zone 1).

6.3 Results and discussion

Figure 13 shows the relative importance of pure diffusion and pure inertial effects in the equation for mass flux (Equation (1)). For all curves in this figure, we assume that the effective roughness height, k_s, is zero, and that the flow is isothermal (no thermal diffusion). The

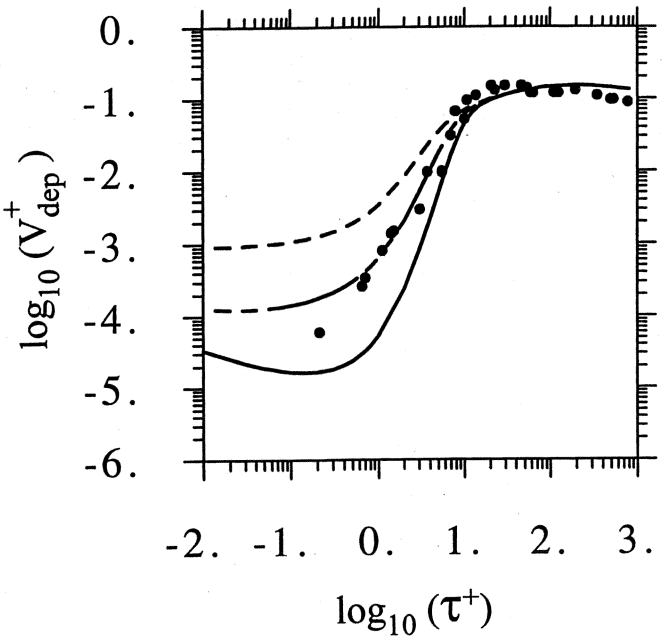

Figure 14. Effects of surface roughness on the predicted deposition rate (without lift force) and comparison with experimental results of Liu and Agarwal (1974).
—— $k_s^+ = 0$, - - — $k_s^+ = 0{\cdot}5$, - - - - $k_s^+ = 1{\cdot}5$, ● experimental results of Liu and Agarwal. For all curves, $\Delta T = 0$.

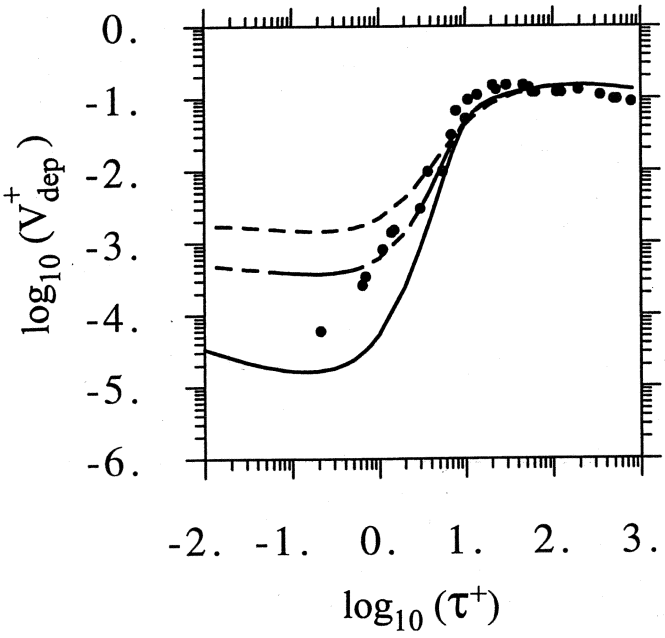

Figure 15. Effects of diffusion due to temperature gradient on the predicted deposition rate (without lift force).
—— $\Delta T = 0$, - - — $\Delta T = 5$ K, - - - -, $\Delta T = 20$ K, ● experimental results of Liu and Agarwal. For all curves, $k_s^+ = 0$.

pure diffusion case is calculated by assuming that the turbulence is homogeneous. The source term in the RHS of Equation (2c) is zero and, consequently, the convective velocity, $\overline{V}^c_{py}$, is zero. Under these circumstances, Equation (1) becomes identical with the turbulent version of Fick's law. As discussed in Section 6.1, the deposition velocity monotonically decreases with increasing relaxation time. This case was calculated by taking the lower boundary at $y^+ = 0$. The behaviour of the deposition velocity, however, changes if one includes the effects of interception. The lower boundary is now at one particle radius away from the wall. As the lower boundary is shifted, the effective resistance against mass transfer tends to decrease. For large relaxation times, this effect can more than offset the effect of lower Brownian diffusion coefficient, D_B. For large relaxation times, the calculated deposition velocity, therefore, increases substantially with increasing relaxation time (Fig. 13), even though the convective velocity, $\overline{V}^c_{py}$, is neglected.

For calculating pure inertial effects, only the third term in the RHS of Equation (1) is retained. Figure 13 shows that the convective velocity goes to zero for very small particles. Its effect on the deposition velocity has become comparable to that of pure diffusion around $\tau^+ \sim 0{\cdot}2$. It then rises steeply by several order of magnitude as τ^+ increases. The solid line in Fig. 13 is calculated by retaining all terms in Equation (1). It merges with the pure diffusion case for very small particles and merges with the pure inertial case for large particles. The relative importance of diffusion, inertia and interception can clearly be appreciated from Fig. 13.

Figure 14 shows the variation in deposition velocity with relaxation time for three different roughness parameters: $k_s^+ = 0$, $k_s^+ = 0{\cdot}5$ and $k_s^+ = 1{\cdot}5$. The Reynolds number and the density ratio (ρ_p°/ρ_f) are taken as 10 000 and 770 respectively, as in Liu and Agarwal's experiments[10]. Equations (1) and (2c) are solved in full form for isothermal flow (no diffusion due to temperature gradient). The effect of roughness is reflected in the calculation procedure through a shift in the lower boundary of the computational domain. As expected, roughness affects the deposition velocity when diffusion is important. In the same figure the experimental data of Liu and Agarwal (1974), which have gained the reputation of one of the most trustworthy measurements, are also plotted for comparison. It can be seen that the present calculation scheme captures all the features of measured deposition velocity both qualitatively as well as quantitatively. Specifically, the calculated curve for $k_s^+ = 0{\cdot}5$ is almost superposed on the experimental values.

Figure 15 shows the effects of temperature gradient on the deposition velocity. Equations (1) and (2c) are solved for three cases: $\Delta T = 0$, $\Delta T = 5$ K and $\Delta T = 20$ K, where ΔT is the temperature difference between the upper boundary of the calculation domain ($y^+ = 200$) and the pipe wall (the wall is cooled). The roughness k_s^+ is assumed zero for all cases. Diffusion due to temperature gradient (second term in the RHS of Equation (1)) is important for small particles. Even a small temperature difference (e.g. $\Delta T = 5$ K) has a significant effect on the deposition velocity. For $1 < \tau^+ < 10$, there is an interaction between thermophoresis and turbophoresis.

6.4 Conclusion

A unified theory of deposition is presented. Given that the deposition velocity varies by more than four order of magnitude in the range of particle sizes under investigation, and that it is calculated from a simple, universal Equation (1) which contains only a modicum of empiricism and no "tuning factor", it is indeed remarkable that the calculated deposition velocity agrees so well with the experimental values.

Present calculations (Fig. 14) show that the presence of small surface roughness even in the hydraulically smooth regime significantly enhances deposition of small particles. Figure 15 shows that thermophoresis can be equally important (and should be considered, for example, in deposition calculations for internally-cooled gas turbine blades). For intermediate size particles, there can be a strong interaction between thermophoresis and turbophoresis.

The effects of different deposition mechanisms come out naturally from the present analysis in a physically satisfying manner and there is scope to add other effects in a straightforward, logical way. The present theory is also logical in finding the combined effects of different deposition mechanisms, as the appropriate forces are added in the momentum equation and the combined "velocity" or flux is calculated by solving the continuity and momentum equations. This should be superior to the often-used linear addition of respective "velocities" in order to determine the combined mass flux (e.g. adding a turbophoretic velocity with a diffusive velocity).

Reference 10 provides the details of the presented theory and shows that this simple theory produces results that are at least as accurate as the most sophisticated state-of-the-art Lagrangian calculations. Being Eulerian, the present theory not only offers a very inexpensive method of computation but also can be readily integrated with established (single-phase) Eulerian flow solvers.

7.0 EPILOGUE

The well-known books on multi-phase flows (e.g. by N.A. Fuchs, by G.B. Wallis or by C.N. Davies) describe the long, inexhaustible list of multi-phase phenomena demonstrating their all-pervasive occurrence. The literature on multiphase flow is therefore vast, a significantly long list may be compiled by combining the lists of references provided in the articles cited in this paper. Here, we have considered only a few important topics, the selection inevitably being biased by the author's own interests. A complementary combination of analytical and computational techniques, and differential and integral treatments has been used in order to model fundamental processes occurring in two-phase mixtures as well as to explain observed phenomena and experimental findings. This is an exciting, rewarding and potent field, so many interesting and important things remain to be done!

REFERENCES

1. GUHA, A. Two-phase flows with phase transition, VKI Lecture Series 1995-06, von Karman Institute for Fluid Dynamics, Belgium, 1995, pp 1-110.
2. GUHA, A. A unified theory of aerodynamic and condensation shock waves in vapour–droplet flows with or without a carrier gas, *Physics Fluids*, 1994, **6**, (5), pp 1893-1913.
3. GUHA, A. Thermal choking due to nonequilibrium condensation, Trans ASME, *J Fluids Eng*, 1994, **116**, pp 599-604.
4. GUHA, A. and YOUNG, J.B. Time-marching prediction of unsteady condensation phenomena due to supercritical heat addition, Proc Conf Turbomachinery: Latest developments in a Changing Scene, London, IMechE, Paper C423/057, 1991, pp 167-177.
5. GUHA, A. Jump conditions across normal shock waves in pure vapour–droplet flows, *J Fluid Mech*, 1992, **241**, pp 349-369.
6. GUHA, A. Structure of partly dispersed normal shock waves in vapour–droplet flows, *Physics Fluids A*, 1992, **4**, (7), pp 1566-1578.
7. GUHA, A. and YOUNG, J.B. Stationary and moving normal shock waves in wet steam, In *Adiabatic Waves in Liquid-Vapour Systems* (MEIER, G.E.A. and THOMPSON, P.A. (Eds)), Springer, 1989, pp 159-170.
8. GUHA, A. and YOUNG, J.B. The effect of flow unsteadiness on the homogeneous nucleation of water droplets in steam turbines, *Phil Trans Royal Soc*, 1994, **349**, pp 445-472.
9. GUHA, A. A unified theory for the interpretation of measured total pressure and total temperature in multiphase flows at subsonic and supersonic speeds, Proc Royal Soc, Series A, 1998, **454**, (1970), pp 671-695.
10. GUHA, A. A unified Eulerian theory of turbulent deposition to smooth and rough surfaces, *J Aerosol Science*, 1997, **28**, (8), pp 1517-1587.